Design and Performance Analysis of Ultra-massive Multi-carrier Multiple Input Multiple Output Communications in the Terahertz Band

Luke M. Zakrajsek, Dimitris A. Pados, and Josep M. Jornet

Department of Electrical Engineering
University at Buffalo, The State University of New York
Buffalo, NY 14260, USA

ABSTRACT

Terahertz (THz)-band communication is envisioned as a key wireless technology to satisfy the need for much higher wireless data rates. To date, major progress in electronic, photonic and plasmonic technologies is finally closing the so-called THz gap. However, the exceedingly large available bandwidth at THz frequencies comes at the cost of a very high propagation loss. Combined with the power limitations of THz transceivers, this results in very short communication distances. Moreover, the absorption by water vapor molecules further splits the THz band in multiple transmission windows, which shrink as the transmission distance increases. To overcome these limitations, the concept of Ultra-Massive Multi-Carrier Multiple Input Multiple Output (UMMC MIMO) communication, which relies on the use of ultra-dense frequency-tunable plasmonic nano-antenna arrays, has been recently proposed. In this paper, the end-to-end performance of a UMMC MIMO link is analytically and numerically investigated. More specifically, an optimization framework is developed to determine the information capacity of UMMC MIMO communication by taking into account both the capabilities of THz plasmonic nano-antenna arrays and the peculiarities of the THz channel. In relation to the arrays, the frequency tunability of each individual element in the transmitter's and receiver's plasmonic arrays is taken into account. In terms of the channel, the impact of the spreading loss and the molecular absorption loss is considered. Extensive numerical results are provided to illustrate the performance of the proposed communication scheme.

Keywords: Terahertz communications, Graphene plasmonics, Ultra-massive MIMO, Ultra-broadband networks

1. INTRODUCTION

Over the past decade, wireless data rates have risen dramatically due to major technology advancements and changes in the way society creates, shares and consumes information. By one estimate, wireless data rates have roughly doubled every eighteen months over the past decades.[1] However, there are serious limitations in currently used wireless technologies that will prevent this trend from continuing unhindered, and which motivate the search for completely new communication paradigms. While millimeter-wave solutions[2,3] can provide short term relief, a long-term more ambitious goal is the implementation of Terahertz (THz)-band (0.1 THz to 10 THz) communication.[4,5] The use of the THz band for communication has long been a challenge due to the lack of compact devices able efficiently generate, modulate, radiate, detect and demodulate THz signals at room temperature. Today, new nano-engineering tools and materials are finally closing the THz gap.[6,7]

Among others, one of the most promising methods to enable THz communications relies on the use of graphene-based nano-transceivers and nano-antennas. The unique electrical properties of graphene, such as its very high electron mobility, make it ideal for supporting extremely high frequency signals.[8,9] Among others, graphene supports the propagation of surface plasmon polariton (SPP) waves at THz frequencies.[10,11] An SPP

Further author information: (Send correspondence to L.M.Z)
L.M.Z.: E-mail: lukezakr@buffalo.edu
D.A.P.: E-mail: pados@buffalo.edu
J.M.J.: E-mail: jmjornet@buffalo.edu

Image Sensing Technologies: Materials, Devices, Systems, and Applications IV,
edited by Nibir K. Dhar, Achyut K. Dutta, Proc. of SPIE Vol. 10209, 102090A
 · doi: 10.1117/12.2264424

wave is a confined electromagnetic wave coupled to the electric charges between a metal and a dielectric. Hybrid structures based on III-V semiconductor materials can be used to excite THz SPP waves on graphene,[12] and graphene-based resonant plasmonic cavities can be utilized to radiate them.[13] In addition, graphene-based nano-antennas provide added advantages such as electrical tunability[14] and reconfigurability.[15] Furthermore, graphene-based plasmonic nano-antennas can be integrated into very dense plasmonic nano-antenna arrays. On the one hand, the use of nano-antenna arrays is needed to increase the limited power of individual plasmonic sources (expectedly $<10\,\mu W$) through beamforming. On the other hand, the capabilities of THz nano-antennas and the peculiarities of the THz-band channel introduce new considerations in array design not present at lower frequencies, which enable new communication schemes that can lead to practical THz communication systems.

In this direction, the concept of Ultra-Massive Multiple-Input Multiple-Output (UM MIMO) communication has been recently proposed.[16] In UM MIMO, compact very dense plasmonic nano-antenna arrays (e.g., 1024 elements in $1\,mm^2$ at 1 THz) are simultaneously utilized in transmission and reception (e.g., 1024x1024 MIMO) to increase the communication distance and, ultimately, the achievable data-rates at THz frequencies. UM MIMO supports different communication schemes, ranging from UM beamforming with razor-sharp beams, to UM spatial multiplexing for high spatial reuse. In addition, the possibility to tune different nano-antennas at different frequency windows within the THz band, enables UM Multi-Carrier MIMO systems (UMMC MIMO). UMMC MIMO communication can expectedly maximize the utilization of the THz band by simultaneously focusing the transmitted signal in space (beamforming) and in frequency (absorption-free transmission windows).

In this paper, we analytically and numerically investigate the end-to-end performance of a UMMC MIMO link. More specifically, first, we summarize the properties of graphene plasmonic nano-antennas and nano-antenna arrays (Section 2). Then, we review the peculiarities of the THz channel and, in particular, the impact of molecular absorption on the available transmission bandwidth (Section 3). Motivated by these results, we describe the working principle of UM MC MIMO communications and formulate a mathematical framework to analyze the capacity of such system (Section 4). Finally, extensive numerical results, backed up by electromagnetic device simulations, are provided to illustrate the potential of this communication technique (Section 5). The results show that a UMMC MIMO link provides significant capacity improvements over that of a single frequency system, with over 10 Tbps at a link distance of one meter and up to 8 Tbps at a link distance of ten meters.

2. GRAPHENE BASED PLASMONIC NANO-ANTENNA ARRAYS

Plasmonic nano-antenna arrays have been recently proposed as a mechanism to overcome the very high path-loss at THz frequencies.[16] In addition to their intrinsic compatibility with THz plasmonic sources,[12,17] graphene-based plasmonic nano-antennas and nano-antenna arrays exhibit several advantageous properties when compared to conventional metallic antennas and antenna arrays. Therefore, in order to compute the information capacity of a UMMC MIMO THz communication link, it is necessary to understand and capture the unique properties provided at the device level.

The first step to derive the properties of graphene-based nano-antennas requires us to determine the conductivity of graphene. In our analysis, we adopt the surface conductivity model for infinitely large graphene sheets given by[18,19]

$$\sigma^g = \sigma^g_{\text{intra}} + \sigma^g_{\text{inter}}, \tag{1}$$

$$\sigma^g_{\text{intra}} = i\frac{2e^2}{\pi\hbar^2}\frac{k_B T}{\omega + i\tau_g^{-1}} \ln\left(2\cosh\left(\frac{E_F}{2k_B T}\right)\right), \tag{2}$$

$$\sigma^g_{\text{inter}} = \frac{e^2}{4\hbar}\left(H\left(\frac{\omega}{2}\right) + \mathrm{i}\frac{4\omega}{\pi}\int_0^\infty \frac{H(\epsilon) - H(\omega/2)}{\omega^2 - 4\epsilon^2}\, d\epsilon\right), \tag{3}$$

with

$$H(a) = \frac{\sinh\left(\hbar a/k_B T\right)}{\cosh\left(E_F/k_B T\right) + \cosh\left(\hbar a/k_B T\right)}, \tag{4}$$

where $\omega = 2\pi f$ is the angular frequency, $\hbar = h/2\pi$ is the reduced Planck's constant, e is the electron charge, k_B is the Boltzmann constant, T is temperature, τ_g is the relaxation time of electrons in graphene, and E_F refers to the Fermi energy of the graphene sheet.

Second, the characteristic length of a graphene-based plasmonic nano-antenna is determined by the plasmonic wave number, k_{spp}, which is obtained by solving the SPP wave dispersion equation on the specific graphene heterostructure. As first described in,[13] a graphene-based plasmonic nano-antenna consists of a graphene layer (the active element) on top of a metallic ground plane with a dielectric layer in between. The ground plane is required both to define a resonant cavity for SPP waves as well as to serve as a back gate to control the Fermi energy of the graphene layer. From,[20] the dispersion equation for Transverse Magnetic (TM) SPP waves in gated graphene structures in the quasi-static regime—i.e., for $k_{spp} \gg \omega/c$—is given by

$$-i\frac{\sigma^g}{\omega\varepsilon_0} = \frac{\varepsilon_1 + \varepsilon_2 \coth(k_{spp}d)}{k_{spp}}, \tag{5}$$

where σ^g is the conductivity of graphene (1), ε_1 is the relative permittivity of the dielectric above the graphene layer, and ε_2 is the relative permittivity of the dielectric between the graphene layer and the metallic ground plane. A closed-form expression for the SPP wave vector k_{spp} does not exist and, thus, the dispersion equation needs to be solved for k_{spp} numerically.

Finally, the characteristic resonant length for the fundamental TM mode of the nano-antenna is given by

$$L = \frac{\lambda_{spp}}{2} = \frac{\pi}{Re\{k_{spp}\}}, \tag{6}$$

where λ_{spp} is the SPP wavelength. In,[13] we showed that k_{spp} is highly confined (i.e., $k_{spp} \ll k$, where k is the wave vector in free space), leading L to be up to two orders of magnitude smaller than that of a conventional microstrip antenna at THz frequencies. In addition, in our previous work in,[21] we showed analytically and through simulation that the magnitude of the mutual coupling experienced by adjacent nano-antennas is similarly determined by SPP wavelength, as opposed to the free-space wavelength. The combination of these two properties allows the design of ultra-dense plasmonic arrays with nano-antennas at spacings close to the SPP wavelength.

The relationship between a plasmonic nano-antenna and its corresponding source results in another departure from conventional antenna theory. Typically an antenna array is fed from a single or a limited number of sources, and so the available output power per antenna is a function of the power from the source and the total number of elements in the array. In contrast, a plasmonic array connects a single source to each nano-antenna. In this case, each antenna-source pair is truly an active element, and the available power of each antenna is independent of the total number of elements, or in other words, the total power of the system is dependent on the total number of active antennas. In this design, there is an extra benefit to increasing the number of elements in the array besides the usual benefits of increased directivity and beamforming. Ultra-dense spacing and individual sources can enable a UMMC MIMO system when combined with the ability of graphene to provide electronic tunability.

Graphene is tunable, as investigated in,[14,22] and this tunability can be leveraged to design a graphene based nano-antenna array where different elements are tuned to resonate at different frequencies using voltage biasing. By changing the Fermi energy of the graphene layer, the SPP confinement factor changes and, thus, the resonance frequency of the nano-antenna is modified. For example, in Figure 1(a) we illustrate the impact of the Fermi energy on the resonance frequency of a graphene-based plasmonic nano-antenna with $L = 3$ μm and using a SiO_2 dielectric ($\varepsilon_r = 4$) with a thickness of 90 nm between the graphene layer and the ground plane. As a result, multiple THz band carrier frequencies can be supported within the same array without changing any physical parameters. To illustrate this behavior, in Figure 1(b), the radiated power is shown from a sixteen element graphene based nano-antenna array with uniform spacing of $\lambda_{spp} = \lambda/25$, with eight antennas tuned to $E_F = 0.2$ eV and four antennas tuned to $E_F = 0.4$ eV. The ease of supporting multiple carrier frequencies, the active nature of the graphene-based nano-antennas, and the ability for ultra-dense spacing are characteristics inherent to a graphene-based nano-antenna array that we will leverage to fully exploit the THz-band communication channel.

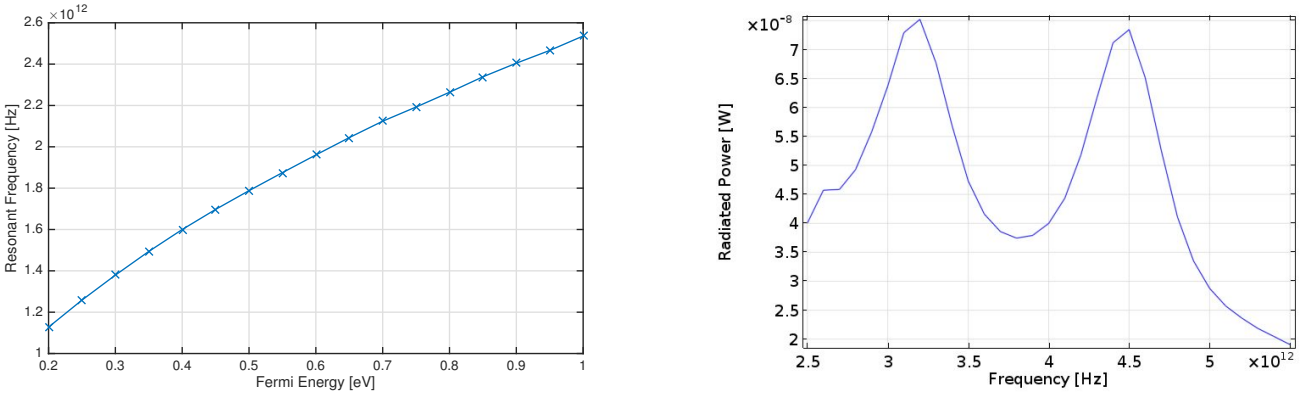

Figure 1. a) Graphene resonance frequency dependence on Fermi energy for an antenna of length 3 μm. b) Graphene-based array with uniform length nano-antennas resonating at multiple frequencies simultaneously.

3. THE TERAHERTZ-BAND CHANNEL

In addition to the capabilities of THz plasmonic devices, the peculiarities of the THz-band channel further motivate and impact the performance of UM MC MIMO systems. There have been several recent works aimed at analytically modeling the path-loss at THz frequencies both for line-of-sight (LoS)[23,24] and non-line-of-sight (NLoS)[25,26] propagation conditions. In our analysis, we focus on LoS propagation and consider the impact of reflected, scattered and reflected rays to be negligible provided that the direct path is not blocked.[25] From,[23] the path-loss or attenuation for LoS is contributed by both the spreading loss and the molecular absorption loss, and is given by

$$\alpha_{LoS}(f) = \left(\frac{c}{4\pi R f}\right) exp\left(-\frac{1}{2}\mathcal{K}(f)R\right) exp(-j2\pi f \tau_{LoS}), \tag{7}$$

where f stands for frequency, c is the speed of light, R is the link distance and $\tau_{LOS} = R/c$ stands for the time of arrival. The term $\mathcal{K}$ refers to the molecular absorption coefficient and accounts for the loss of energy experienced by the signal due to the molecules in the medium converting a fraction of the wave electromagnetic energy into kinetic vibrational energy. The molecular absorption coefficient is a function of frequency and can be written as

$$\mathcal{K}(f) = \sum_i \frac{\zeta}{\zeta_0}\frac{T_{STP}}{T}\Omega^i \xi^i(f), \tag{8}$$

where ζ is the system pressure, T is the temperature in Kelvin, ζ_0 is the reference pressure, T_{STP} is the temperature at standard pressure, Ω^i is the number of molecules per unit of gas i, and ξ^i is the absorption cross-section of gas i at THz frequencies. Full details on how to compute the absorption cross section, by using radiative transfer theory and the information in the HITRAN database, can be found in Ref.[23]

The attenuation due to molecular absorption defines multiple absorption spikes at various frequencies corresponding to where molecules become resonant and, consequently, multiple transmission windows in between these spikes (see Figure 2). In Table 1, we list the center frequency f_c, 3dB bandwidth B_{3dB}, absorption loss A_{abs} and total path-loss A for the 3 dB windows at 10 m whose bandwidth is larger than 20 GHz. In a strict sense, there is an initial window, w_0, from 275 GHz to 380 GHz, lower bounded by regulations and upper bounded by absorption. While there are some absorption peaks in between, they are not significant at 10 m.

Traditionally, the absorption loss is given as a magnitude in dB/km at a given window. However, this masks the fact that the absorption loss also determines the bandwidth, which changes drastically with distance. As the distance increases, or, respectively, the number of absorbing molecules augments, not only the absorption loss increases, but the transmission windows shrink. This requires the development of dynamic systems able to cope with the distance-changing bandwidth and, thus, motivates the development of UMMC MIMO communication.

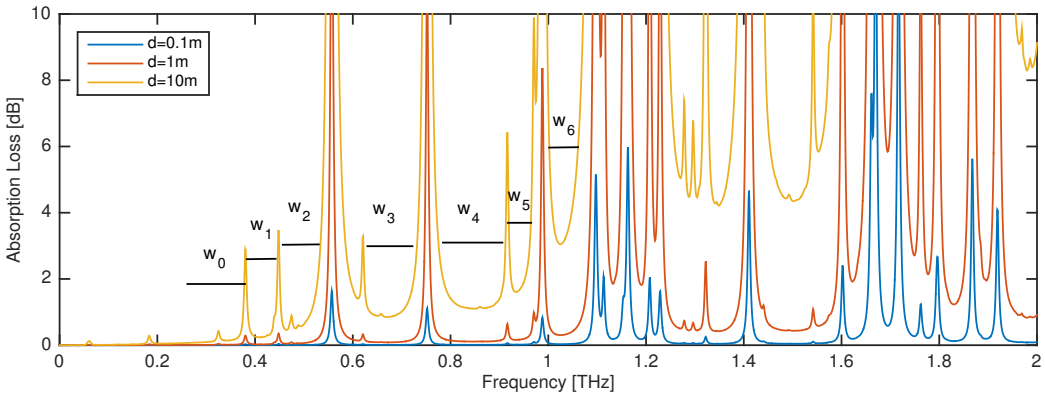

Figure 2. Molecular absorption loss in dB at different transmission distances.

Table 1. 3dB absorption windows at 10 m

Name	f_c [THz]	B_{3dB} [GHz]	A_{abs} [dB]	A [dB]	Name	f_c [THz]	B_{3dB} [GHz]	A_{abs} [dB]	A [dB]
w_1	0.41	65.61	0.24	105.02	w_7	1.3	38.15	4.46	121.39
w_2	0.49	86.21	0.46	106.86	w_8	1.35	51.12	4.21	119.41
w_3	0.66	152.59	0.85	109.76	w_9	1.49	91.55	4.34	120.47
w_4	0.84	141.91	1.10	112.07	w_{10}	1.56	28.99	5.84	122.37
w_5	0.94	47.3	1.61	113.62	w_{11}	1.83	25.18	12.31	130.03
w_6	1.03	57.98	3.05	115.85	w_{12}	1.98	56.46	8.30	126.69

4. CAPACITY OF UMMC MIMO COMMUNICATION

In this section, we first describe the working principle and rationale for the design of UMMC MIMO systems and then we mathematically formulate an optimization framework to compute the achievable information capacity.

4.1 UMMC MIMO System Configuration

In the proposed UMMC system, the transmitter and the receiver are comprised of a graphene-based plasmonic nano-antenna array. Each nano-antenna is individually powered and controlled, as described in Section 2. The resulting arrays can be tuned to operate at one or multiple absorption-defined transmission windows described in Section 3, which enables the transmission of simultaneous data streams at different frequencies.

The allocation of the nano-antennas to different frequencies is not a trivial problem. Let us consider an array with a fixed total number of nano-antennas, fixed separation between them and, thus, occupying a fixed footprint. On the one hand, all the nano-antennas could be tuned to operate at the same frequency, thus, working in a very similar way as in traditional MIMO schemes and enabling ultra-massive beamforming schemes for maximum gain. On the other hand, each nano-antenna could be allocated to a different carrier frequency, thus, maximizing the spectrum utilization at the cost of a lower gain per frequency. As we will illustrate in the next section, there is an optimal allocation of the antennas that maximizes the capacity. When allocating the nano-antennas at different frequencies, the properties of plasmonic nano-antenna arrays need to be taken into account. As discussed in Section 2, the minimum separation between plasmonic nano-antennas is on the order of a full plasmonic wavelength, i.e., much smaller than the traditional half free-space wavelength. While this allows the dense packaging of the nano-antennas, it limits the beamforming gain of the array due to inadequate spatial sampling. For this, instead of allocating contiguous nano-antennas to the same frequency, nano-antennas at different frequencies are interleaved along both axes. Fig. 3 illustrates the interleaving scheme for one, two, and four carrier frequencies. Ideally, the separation between two adjacent elements tuned at the same carrier frequency should never be more than $\lambda/2$ to maximize the beamforming gain and minimize side lobes. However, the minimum separation can be much smaller. Consequently, the number of possible carrier frequencies is upper bounded by the number of nano-antennas which can fit within $\lambda/2$ in order to satisfy the given constraints.

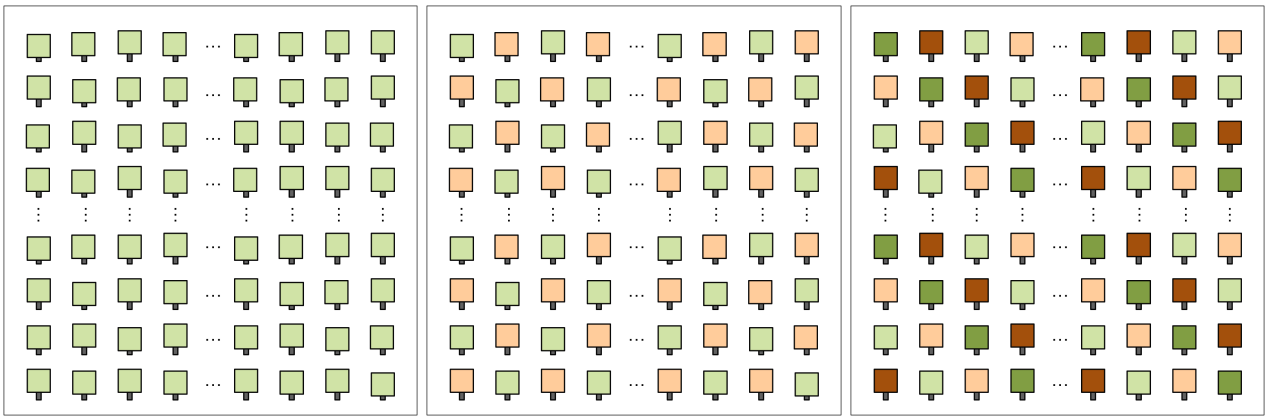

(a) 1 Frequency (b) 2 Frequencies (c) 4 Frequencies

Figure 3. Structure of UMMC MIMO array showing three possible interleaving layouts for the same array.

4.2 UMMC MIMO Capacity Formulation

The maximum achievable information rate or capacity of the proposed UMMC MIMO communication system can be obtained by solving a resource allocation problem. The objective is to determine how many absorption-defined transmission windows to utilize and how many nano-antennas need to be tuned per frequency window so to maximize the aggregated capacity over the entire band. The problem is formulated as follows:

Given:

$$N_{t,r}, W, D, P_t, R, G(\theta,\phi)_{antenna}, \tag{9}$$

$$F = [f_1, f_2, f_3, ...f_W]^T, \tag{10}$$

$$B = [b_1, b_2, b_3, ...b_W]^T, \tag{11}$$

Find:

$$w \tag{12}$$

Maximize:

$$Capacity = \sum_{j=1}^{w} B_j \log_2 \left(1 + \frac{P_{r,j}}{N_{0,j}}\right) \tag{13}$$

Subject To:

$$N_t = N_r = N_m \times N_m, \tag{14}$$

$$n_{t,r} = \frac{N_{t,r}}{w}, \tag{15}$$

$$P_{r,j} = P_t G_{r,j} G_{t,j} \alpha_{LoS}(f_j), \tag{16}$$

$$G_{t,j}, G_{r,j} = max(G(\theta,\phi)^{t,r}_{antenna} \times G(\theta,\phi)^{t,r}_{array,j}), \tag{17}$$

$$G(\theta,\phi)^{t,r}_{array,j} = \mathcal{AF}_j\left(\theta,\phi\right)^2, \tag{18}$$

$$\tag{19}$$

$$\mathcal{AF}_j\left(\theta,\phi\right) = \left(\frac{\sin\left(n\frac{\psi_{x,j}}{2}\right)}{\sin\left(\frac{\psi_{x,j}}{2}\right)}\right)\left(\frac{\sin\left(n\frac{\psi_{y,j}}{2}\right)}{\sin\left(\frac{\psi_{y,j}}{2}\right)}\right), \tag{20}$$

$$\psi_{x,j} = \frac{2\pi D}{\lambda_j}\sin\theta\cos\phi - \frac{2\pi D}{\lambda_j}\sin\theta_0\cos\phi_0, \tag{21}$$

$$\psi_{y,j} = \frac{2\pi D}{\lambda_j}\sin\theta\sin\phi - \frac{2\pi D}{\lambda_j}\sin\theta_0\sin\phi_0, \tag{22}$$

$$\alpha_{LoS}(f_j) = \left(\frac{\lambda_j}{4\pi R}\right) exp\left(-\frac{1}{2}\mathcal{K}(f_j)R\right) exp(-2j\pi f_j\tau_{LoS}), \tag{23}$$

$$\mathcal{K}(f_j) = \sum_i \frac{\zeta}{\zeta_0}\frac{T_{STP}}{T}\Omega^q\xi^q(f_j), \tag{24}$$

where:

- Both transmit and receive antennas are square planar and given by size $N_m \times N_m$, where N_m is the number of antennas along one axis.
- $N_{t,r}$ are the total number of transmit and receive antennas respectively, D is the uniform distance between any two adjacent antennas along the x or y axis, P_t is the transmit power of one antenna, R is the communication distance, and $G(\theta,\phi)^{t,r}_{antenna}$ is the gain of one antenna element.
- W is the total number of available frequency windows in the THz band, F is the corresponding center frequency vector, and B is the corresponding bandwidth vector.
- $n_{t,r}$ are the total number of antennas used for each carrier frequency for the transmit and receive antennas, respectively.
- w is the number of carrier frequencies in use by the array.
- P_r is the received power, which is a function of the transmit power P_t, the gain of the receiving link and the transmitting link given by $G_{r,j}$ and $G_{t,j}$, and the line of sight attenuation given by $\alpha_{LoS}(f_j)$.
- The gain of the receiver and the gain of the transmitter are given by the gain of the individual antenna multiplied by the gain contributed by the array, which is computed through the antenna factor $\mathcal{AF}_j\left(\theta,\phi\right)$. Both are functions of θ and ϕ, which are the azimuth angle and the elevation angle, respectively.
- The antenna factor $\mathcal{AF}_j\left(\theta,\phi\right)$ includes the terms $\psi_{x,j}$ and $\psi_{y,j}$. These take into account λ_j, the wavelength of the center frequency, d, the distance between adjacent elements, and θ_0 and ϕ_0, which are the pointing angles in the azimuth and elevation planes.
- The LoS attenuation takes into account both the molecular absorption function $\mathcal{K}(f_j)$ and the spreading loss, which is related to the carrier frequency.
- In the molecular absorption function $\mathcal{K}(f_j)$ consists of the system pressure ζ, the temperature T, the reference pressure ζ_0, the number of molecules per volume unit of gas Ω^i, and the absorption cross section of gas at THz frequencies, $\xi^i(f_j)$

5. NUMERICAL RESULTS

Using the mathematical framework for UMMC nano-antenna arrays described in Section 4, the capacity of the system and its dependence on the assignment of carrier frequencies is obtained for a number of realistic array configurations. In particular, this relationship is shown for communication distances of one meter and ten meters, and for nano-antenna separation distances D of $\lambda/8$, $\lambda/32$, and $\lambda/128$ and total number of elements per array axis N_m ranging from 16 to 128.

In order to accurately take into account the physical properties of plasmonic nano-antenna arrays, values for the antenna radiated power and antenna gain were taken from full wave frequency domain simulations performed using COMSOL Multi-physics.[27] Graphene is modeled as a transition boundary condition with complex dynamic conductivity given by (1), where $\tau_g = 0.5\,\text{ps}$ and $E_F = 0.4\,\text{eV}$ at $T = 300\,\text{K}$. These values are based on analysis of Raman spectra obtained from CVD-grown graphene.[28] The antenna is fed with a lumped port that connects the graphene layer to the ground plane on one side, and a perfectly matched layer and a scattering boundary condition are utilized to minimize the impact of simulating a finite space. From the COMSOL simulations, the antenna transmit power used for the capacity calculations is $P_t = 100\,\text{nW}$ and the maximum gain of one antenna element is $G_{antenna}$=6.5 dB. In addition, the noise considered consists of the thermal noise and the molecular absorption noise generated by transmission in a channel of standard medium composition with 10% water vapor molecules. Capacity is solved for by exhaustive search for available transmission windows in the THz band, and then using the window with the highest available capacity each time a new carrier frequency is added.

The results illustrate the benefit of operating at multiple carrier frequencies in order to utilize the available THz frequency windows. Figure 4 shows the capacity for a number of nano-antenna arrays, each with a different number of total elements, but with the element to element spacing held constant at $\lambda/8$. It is shown that a multi-Tbps link can be supported with the proposed UMMC array for distances of ten meters or less, but only if the size of the array is at least 32 x 32 elements at a distance of one meter and at least 64 x 64 elements at a distance of 10 m. It is also clear that the division of the array into interleaved elements provides a significant increase in the information capacity, and the improvement increases with the size of the array.

In Figure 5, it is shown that this trend continues when the element to element spacing is decreased to $\lambda/32$, which allows for a maximum of 16 different carrier frequencies per $\lambda/2$. At communication distances of one meter, the capacity trend appears to continue upward or at least stay constant with increasing number of carrier frequencies. However, at a distance of ten meters the capacity reaches a maximum for the arrays smaller than 256 x 256 before the maximum number (16) of potential frequencies is reached. This is intuitive when the effect of splitting the array is considered in relation to (13). Every time a frequency is added, an extra bandwidth window is added. However, at the same time there are less active antennas contributing power to each frequency. When the available power in each frequency window decreases enough that it is comparable to the noise power, then capacity begins to decrease due to power loss faster than the increase due to greater bandwidth.

To see an even clearer trend, we ignore the physical size and mutual coupling constraints of the antennas and approximate them as point sources in order to decrease the antenna to antenna spacing even further, to $\lambda/256$. With a maximum of 128 interleaved elements per $\lambda/2$, it is clear from Figure 6 that the potential capacity has an optimal point for every size of array considered, illustrating the tradeoff between carrier frequency and antenna power. However, a separation length of $\lambda/256$ is not only well below the free space wavelength but also well below the plasmonic wavelength, and therefore much smaller than the physical size of a plasmonic antenna. While this case is included to make the trend clear, it is expected that the size of plasmonic nano-antennas will be the constraint on the maximum number of carrier frequencies before the transmit power of each frequency becomes a limiting factor.

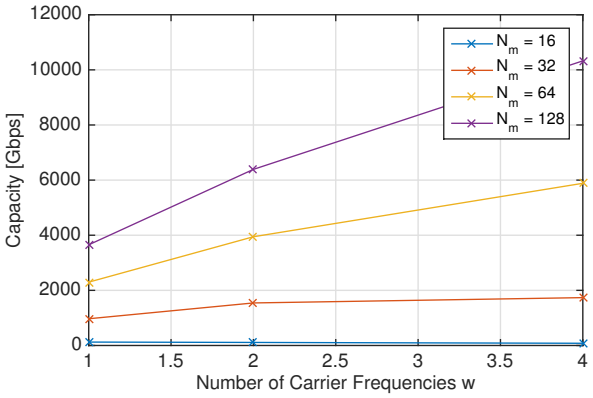

(a) $R = 1\,\mathrm{m}$

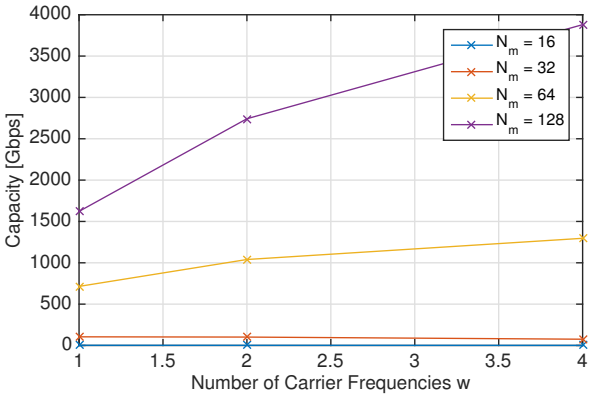

(b) $R = 10\,\mathrm{m}$

Figure 4. Capacity of UMMC MIMO communication (13), for different total number of elements per array axis N_m and fixed element to element spacing $D = \lambda/8$, at two different link distances R.

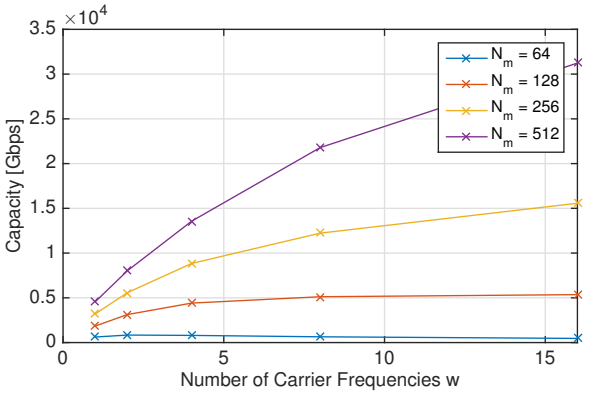

(a) $R = 1\,\mathrm{m}$

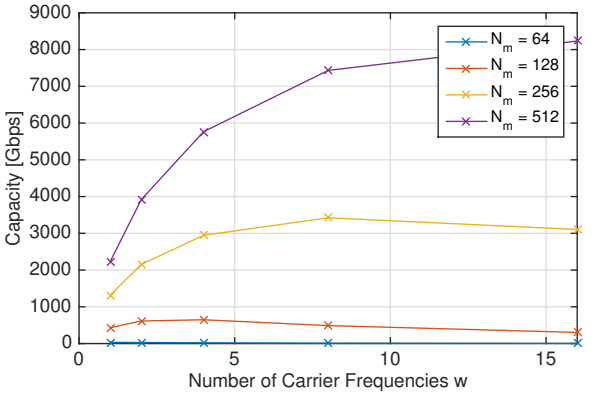

(b) $R = 10\,\mathrm{m}$

Figure 5. Capacity of UMMC MIMO communication (13), for different total number of elements per array axis N_m and fixed element to element spacing $D = \lambda/32$, at two different link distances R.

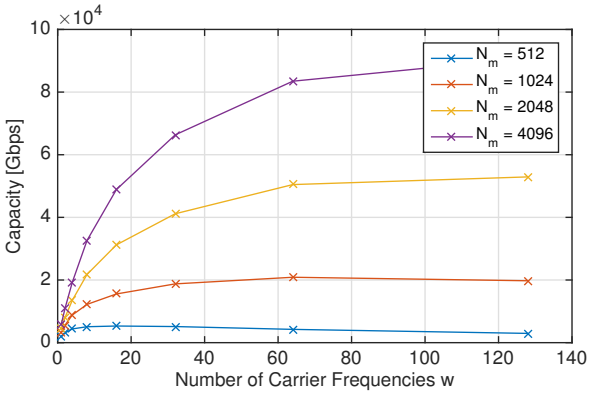

(a) $R = 1\,\mathrm{m}$

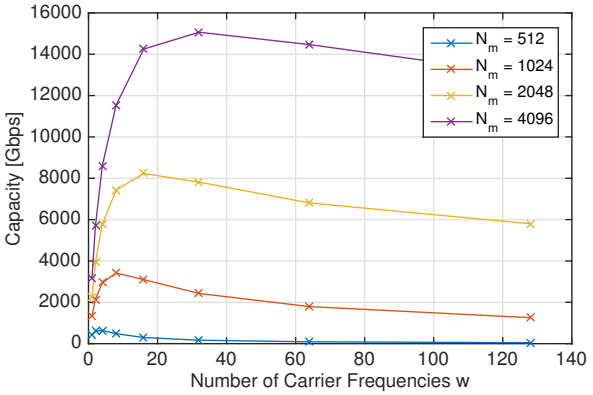

(b) $R = 10\,\mathrm{m}$

Figure 6. Capacity of UMMC MIMO communication (13), for different total number of elements per array axis N_m and fixed element to element spacing $D = \lambda/256$, at two different link distances R.

6. CONCLUSION

In this paper, we have proposed and modeled the performance of Ultra-Massive Multi-Carrier MIMO array design for communication in the THz band. This UMMC MIMO system simultaneously overcomes the problems of limited transmit power of THz sources and molecular absorption loss at THz frequencies while taking advantage of graphene-based plasmonic nano-antenna properties and multiple absorption-loss-defined transmission windows in the THz band. Starting from accurate models of graphene-based plasmonic nano-antenna arrays and the THz-band channel in LoS conditions, a resource allocation problem is formulated to compute the capacity of UMMC MIMO communications. The numerical results, backed-up by full-wave simulations of the supporting devices, highlight the potential of this technique to support multi-Tbps links for practical communications distance beyond several meters, and motivate the development of dynamic algorithms able to solve the resource allocation problem in real-time.

ACKNOWLEDGMENTS

This work was partially supported by the Air Force Office of Scientific Research (AFOSR) under Grant FA9550-16-1-0188. Luke M. Zakrajzek further acknowledges the support of the National Science Foundation Graduate Research Fellowship (Award No. 75773).

REFERENCES

[1] Cherry, S., "Edholm's law of bandwidth," *IEEE Spectrum* **41**, 58 – 60 (July 2004).

[2] Rappaport, T. S., Murdock, J. N., and Gutierrez, F., "State of the art in 60-ghz integrated circuits and systems for wireless communications," *Proceedings of the IEEE* **99**(8), 1390–1436 (2011).

[3] Rangan, S., Rappaport, T. S., and Erkip, E., "Millimeter-wave cellular wireless networks: Potentials and challenges," *Proceedings of the IEEE* **102**(3), 366–385 (2014).

[4] Akyildiz, I. F., Jornet, J. M., and Han, C., "Terahertz band: Next frontier for wireless communications," *Physical Communication (Elsevier) Journal* **12**, 16 – 32 (Sept. 2014).

[5] Kurner, T. and Priebe, S., "Towards THz Communications-Status in Research, Standardization and Regulation," *Journal of Infrared, Millimeter, and Terahertz Waves* **35**(1), 53–62 (2014).

[6] Radisic, V., Leong, K., Scott, D., Monier, C., Mei, X., Deal, W., and Gutierrez-Aitken, A., "Sub-millimeter wave inp technologies and integration techniques," in [*IEEE MTT-S International Microwave Symposium (IMS)*], 1–4 (May 2015).

[7] Slivken, S. and Razeghi, M., "High power, electrically tunable quantum cascade lasers," in [*SPIE OPTO*], 97550C–97550C, International Society for Optics and Photonics (2016).

[8] Novoselov, K. S., Fal, V., Colombo, L., Gellert, P., Schwab, M., Kim, K., et al., "A roadmap for graphene," *Nature* **490**(7419), 192–200 (2012).

[9] Ferrari, A. C., Bonaccorso, F., Fal'Ko, V., Novoselov, K. S., Roche, S., Bøggild, P., Borini, S., Koppens, F. H., Palermo, V., Pugno, N., et al., "Science and technology roadmap for graphene, related two-dimensional crystals, and hybrid systems," *Nanoscale* **7**(11), 4598–4810 (2015).

[10] Ju, L., Geng, B., Horng, J., Girit, C., martin, M., Hao, Z., Bechtel, H., Liang, X., Zettl, A., Shen, Y. R., and Wang, F., "Graphene plasmonics for tunable terahertz metamaterials," *Nature Nanotechnology* **6**, 630–634 (Sept. 2011).

[11] Koppens, F. H. L., Chang, D. E., and Garcia de Abajo, F. J., "Graphene plasmonics: a platform for strong light matter interactions," *Nano Letters* **11**, 3370–3377 (Aug. 2011).

[12] Jornet, J. M. and Akyildiz, I. F., "Graphene-based plasmonic nano-transceiver for terahertz band communication," in [*Proc. of European Conference on Antennas and Propagation (EuCAP)*], (2014).

[13] Jornet, J. M. and Akyildiz, I. F., "Graphene-based plasmonic nano-antenna for terahertz band communication in nanonetworks," *IEEE JSAC, Special Issue on Emerging Technologies for Communications* **12**, 685–694 (Dec. 2013).

[14] Llatser, I., Kremers, C., Cabellos-Aparicio, A., Jornet, J. M., Alarcon, E., and Chigrin, D. N., "Graphene-based nano-patch antenna for terahertz radiation," *Photonics and Nanostructures - Fundamentals and Applications* **10**, 353–358 (Oct. 2012).

[15] Tamagnone, M., Gomez-Diaz, J. S., Mosig, J. R., and Perruisseau-Carrier, J., "Reconfigurable terahertz plasmonic antenna concept using a graphene stack," *Applied Physics Letters* **101**(21), 214102 (2012).

[16] Akyildiz, I. F. and Jornet, J. M., "Realizing ultra-massive mimo (1024× 1024) communication in the (0.06–10) terahertz band," *Nano Communication Networks* **8**, 46–54 (2016).

[17] Ryzhii, V., Ryzhii, M., Mitin, V., and Otsuji, T., "Toward the creation of terahertz graphene injection laser," *Journal of Applied Physics* **110**(9), 094503 (2011).

[18] Falkovsky, L. and Varlamov, A. A., "Space-time dispersion of graphene conductivity," *The European Physical Journal B* **56**, 281–284 (2007).

[19] Hanson, G. W., "Dyadic Green's functions and guided surface waves for a surface conductivity model of graphene," *Journal of Applied Physics* **103**(6), 064302 (2008).

[20] Ryzhii, V., "Terahertz plasma waves in gated graphene heterostructures," *Japanese journal of applied physics* **45**(9L), L923 (2006).

[21] Zakrasjek, L., Thawdar, N., Medley, M., and Jornet, J. M., "Design of graphene-based plasmonic nano-antenna arrays in the presence of mutual coupling," in [*Antennas and Propagation (EuCAP), 2017 11th European Conference on*], IEEE (2017).

[22] Singh, P. K., Aizin, G., Thawdar, N., Medley, M., and Jornet, J. M., "Graphene-based plasmonic phase modulator for terahertz-band communication," in [*Antennas and Propagation (EuCAP), 2016 10th European Conference on*], 1–5, IEEE (2016).

[23] Jornet, J. M. and Akyildiz, I. F., "Channel modeling and capacity analysis of electromagnetic wireless nanonetworks in the terahertz band," *IEEE Transactions on Wireless Communications* **10**, 3211–3221 (Oct. 2011).

[24] Federici, J. F., Ma, J., and Moeller, L., "Review of weather impact on outdoor terahertz wireless communication links," *Nano Communication Networks* **10**, 13–26 (2016).

[25] Han, C., Bicen, A. O., and Akyildiz, I., "Multi-ray channel modeling and wideband characterization for wireless communications in the terahertz band," *IEEE Transactions on Wireless Communications* **14**, 2402–2412 (May 2015).

[26] Priebe, S. and Kurner, T., "Stochastic modeling of THz indoor radio channels," *IEEE Transactions on Wireless Communications* **12**(9), 4445–4455 (2013).

[27] COMSOL Multiphysics Simulation Software, "COMSOL."

[28] Zakrajsek, L., Einarsson, E., Thawdar, N., Medley, M., and Jornet, J. M., "Lithographically defined plasmonic graphene antennas for terahertz-band communication," *IEEE Antennas and Wireless Propagation Letters* **15**, 1553–1556 (2016).